Orbital classification in an N-body bar

Yougang Wang, E. Athanassoula, Shude Mao

Orbital classification in an *N*-body bar

Yougang Wang,[1]★ E. Athanassoula[2] and Shude Mao[1,3,4]

[1]*Key Laboratory of Computational Astrophysics, National Astronomical Observatories, Chinese Academy of Sciences, Beijing 100012, China*
[2]*Aix Marseille Université, CNRS, LAM (Laboratoire d'Astrophysique de Marseille), UMR 7326, F-13388 Marseille 13, France*
[3]*Center for Astrophysics, Department of Physics, Tsinghua University, Beijing 100084, China*
[4]*Jodrell Bank Centre for Astrophysics, University of Manchester, Manchester M13 9PL, UK*

ABSTRACT

The dynamics and evolution of any galactic structure are strongly influenced by the properties of the orbits that constitute it. In this paper, we compare two orbit classification schemes, one by Laskar [numerical analysis of fundamental frequencies (NAFF)], and the other by Carpintero and Aguilar (CA), by applying both of them to orbits obtained by following individual particles in a numerical simulation of a barred galaxy. We find that, at least for our case and some provisos, the main frequencies calculated by the two methods are in good agreement: for 80 per cent of the orbits the difference between the results of the two methods is less than 5 per cent for all three main frequencies. However, it is difficult to evaluate the amount of regular or chaotic bar orbits in a given system. The fraction of regular orbits obtained by the NAFF method strongly depends on the critical frequency drift parameter, while in the CA method the number of fundamental frequencies strongly depends on the frequency difference parameter L_r and the maximum integer used for searching the linear independence of the fundamental frequencies. We also find that, for a given particle, in general the projection of its motion along the bar minor axis is more regular than the other two projections, while the projection along the intermediate axis is the least regular.

Key words: Galaxy: bulge – galaxies: kinematics and dynamics – galaxies: structure.

1 INTRODUCTION

Nearly two-thirds of spiral galaxies in the Universe have a bar structure (e.g. Buta et al. 2010, 2015; Lee et al. 2012). Bars are one of the main drivers for the secular evolution of disc galaxies (see Athanassoula 2013 for a review), and can transport material from the bar region to the centre and redistribute angular momentum within the galaxy. This is emitted by the resonant regions in the bar and its vicinity, and absorbed by the outer parts of the disc and, mainly, by the spheroidal components (halo and bulge). Moreover, there is a strong correlation between the strength of the bar and the amount of angular momentum thus redistributed (Athanassoula 2003). Therefore, understanding the structure and the dynamical properties of bars is one of the most important issues in the formation and evolution of disc galaxies.

Orbits are the fundamental building blocks of any galactic structure and therefore their properties greatly influence those of the structure. Moreover, it is difficult to describe the phase-space distribution for the chaotic orbits, which cannot be adopted to construct torus models (McMillan & Binney 2008). The orbit families and, more generally, the orbital structure in a fixed bar potential have

been considered by many studies (Contopoulos & Papayannopoulos 1980; Zhao 1996; Häfner et al. 2000; Manos & Athanassoula 2011; Wang et al. 2012, 2013). Different methods of orbit classification have been used.

The Lyapunov exponent method (see e.g. Benettin, Galgani & Strelcyn 1976; Benettin et al. 1978, for a description). The Lyapunov exponents describe the time-averaged exponential rate of divergence of two orbits with close initial conditions in the phase space. Orbits with significantly non-zero Lyapunov exponents are chaotic.

The Small ALignment Index method (SALI, Skokos 2001; Voglis, Kalapotharakos & Stavropoulos 2002; Skokos et al. 2004; Carpintero, Muzzio & Navone 2014). This method can be considered as an extension of the Lyapunov one, as it relies on the properties of two arbitrary different initial deviation vectors of an orbit, in order to distinguish efficiently between chaotic and regular orbits. The Generalized ALignment Index (GALI; Skokos, Bountis & Antonopoulos 2007) is similar to SALI, but uses a set of at least three initially linearly independent deviation vectors.

The numerical analysis of fundamental frequencies (NAFF) method relies on the fact that the regular orbits move on a torus-like manifold and are thus quasi-periodic (Laskar 1990, 1993). We will describe it further in Section 3.1.

The spectral analysis method uses the Fourier transform of the time series of each coordinate of a given orbit (Carpintero & Aguilar

1998, hereafter CA98). We will hereafter refer to this method as CA, from the initials of its authors, and describe it further in Section 3.2.

While each method has its advantages, each also suffers from disadvantages. For example, the Lyapunov method necessitates very long integration times and the fraction of chaotic orbits also depends on the integration time (Merritt & Fridman 1996); the SALI method also needs relatively long integration times, albeit much shorter than the Lyapunov method. The CA method has some problems for rotating systems (Carpintero et al. 2003) and depends strongly on the orbit integration time (Wang et al. 2012). Finally, in the NAFF method whether an orbit is regular or not depends on the drift of its frequencies, so that a critical value needs to be adopted (see Section 5 in the present paper). Compared to other methods, CA and NAFF have an important advantage, namely they give more information for the regular orbits, such as their fundamental frequencies, from the ratios of which it is possible to define orbital families. Both of them have been successfully applied to various potential systems (e.g. Papaphilippou & Laskar 1998; Valluri et al. 2010; Bryan et al. 2012; Valluri et al. 2016).

Most studies so far have relied on simple analytic potentials, which, however, are not very realistic. In particular, real bars as well as *N*-body bars are composed of two parts: an inner part which is thick both horizontally and vertically, and an outer part which is thin in both these directions, while as yet no analytical potential with such a property has been developed (see Athanassoula 2016 for a review). *N*-body bar potentials, however, are much more complex to use and there are therefore relatively few studies relying on them, compared to the large number of studies relying on analytic potentials. Manos & Machado (2014) and Machado & Manos (2016) took an intermediate path, using analytical time-dependent potentials modelled after an *N*-body simulation of a strongly barred galaxy. The disadvantage of this approach is that both the disc and the bar potentials are rigid and have not responded to each other, which is not realistic.

An alternative route, much nearer to the *N*-bodies, is to freeze the simulation potential at a representative time and then follow orbits with initial conditions obtained from the positions and velocities of the simulation particles at that chosen time (Athanassoula 2002, 2003, 2005; Martinez-Valpuesta, Shlosman & Heller 2006; Voglis, Harsoula & Contopoulos 2007; Wozniak & Michel-Dansac 2009; Valluri et al. 2012, 2016). This approach has a number of advantages. The corresponding potentials are realistic, and allow for orbital structure studies in bars with a thick inner part and a thin outer part. It also provides a unique and correct definition of the orbital sample which will be used, whereas in rigid potentials this sample is arbitrary, thus rendering any estimate of the fraction of chaos in a given system also entirely arbitrary. Indeed, whether a given orbit is regular or chaotic depends on its location within the galaxy's phase space, and different samples may populate this space differently. This severe drawback of analytical potentials is easily avoided by relying on the simulation to provide the initial conditions of the orbits. Concerning disadvantages, let us mention that a correct description of the potential from the simulation particles is not trivial and also that the potential has been frozen, i.e. does not depend on time. It is nevertheless possible to obtain information on time evolution by considering a series of consecutive times and of corresponding frozen potentials. Thus full time information can be obtained, but in a very time consuming manner.

A third alternative is to use directly the orbits of a preselected number of particles during the simulation (Ceverino & Klypin 2007; Gajda, Lokas & Athanassoula 2015, 2016). This attractively straightforward way has a number of difficulties, not the least being

the fact that most of the available techniques and information on orbital structure have been obtained for non-evolving potentials. As we will show here, however, this third alternative can still be very useful if one chooses carefully the time interval over which one follows the orbits so that it has as little evolution as possible.

In this paper, we will give a detailed comparison of the CA and NAFF orbit classification methods by studying orbits in a simulated bar. The outline of the paper is as follows. In Section 2 we describe briefly our numerically simulated bar. In Section 3 we outline different methods of orbit classifications. In Section 4 we present the main frequencies from two methods. In Section 5 we present the fraction of regular orbits from different classification schemes. In Section 6, we give a brief discussion. In Section 7 we present the summary and conclusions.

2 THE SIMULATION AND BAR ORBITS

The initial conditions of this simulation comprise two components a disc and a halo. Both are live, i.e. described self-consistently, in order to allow exchange of angular momentum and thus a full bar growth (Athanassoula 2002, 2003). The initial density distribution of the disc is

$$\rho_{\rm d}(R, z) = \frac{M_{\rm d}}{4\pi h^2 z_0} \ \exp(-R/h) \ {\rm sech}^2\left(\frac{z}{z_0}\right), \tag{1}$$

where R is the cylindrical radius, h is the disc radial scale length, z_0 is the disc vertical scale thickness and $M_{\rm d}$ is the disc mass. The corresponding numerical values are $h = 3$ kpc, $z_0 = 0.6$ kpc and $M_{\rm d} = 5 \times 10^{10} M_\odot$. For the halo we used an initial volume density of

$$\rho_{\rm h}(r) = \frac{M_{\rm h}}{2\pi^{3/2}} \ \frac{\alpha}{r_{\rm c}} \ \frac{\exp\left(-r^2/r_{\rm c}^2\right)}{r^2 + \gamma^2},$$

where r is the radius, $M_{\rm h}$ is the halo mass, γ and $r_{\rm c}$ are the halo core and cut-off radii, respectively, and the constant α is given by

$$\alpha = \{1 - \sqrt{\pi}q \ \exp(q^2) \ [1 - {\rm erf}(q)]\}^{-1},$$

where $q = \gamma/r_{\rm c}$ (Hernquist 1993). The numerical values used in this run are $r_{\rm c} = 42.4$ kpc, $\gamma = 15$ kpc and $M_{\rm h} = 19.54 \times 10^{10} M_\odot$. The halo is described by 1 million particles and the disc has 200 000 particles.

The initial conditions were built using the iterative method of Rodionov, Athanassoula & Sotnikova (2009), and to run the simulation we used a version of the GADGET3 code kindly made available to us by V. Springel. For a full description of GADGET see Springel, Yoshida & White (2001) and Springel (2005). We adopted a softening length of 100 pc for the disc and of 200 pc for the halo and an opening angle of 0.5.

With these initial conditions, the disc dominates the potential in the inner parts, so that the bar forms very early on in the simulation.

The bar strength is defined as in Athanassoula, Machado & Rodionov (2013). More specifically, the Fourier components of the two-dimensional mass distribution can be written as
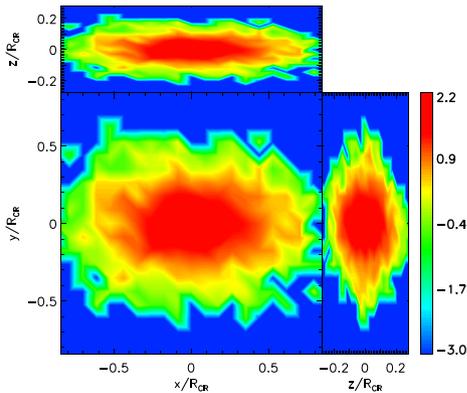
$$a_m(R) = \sum_{i=0}^{N_R} m_i \cos(m\theta_i), \ m = 0, 1, 2, ... \tag{2}$$

$$b_m(R) = \sum_{i=0}^{N_R} m_i \sin(m\theta_i), \ m = 1, 2, ... \tag{3}$$

where N_R is the number of the particles inside a given annulus around the cylindrical radius R, m_i is the ith particle mass and θ_i
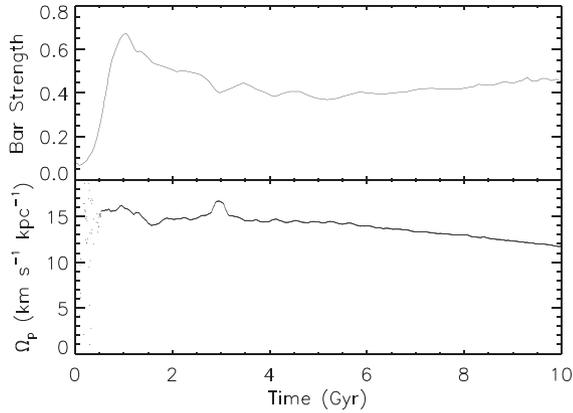
Figure 1. Evolutions with time of the bar strength (top) and pattern speed (bottom) in our *N*-body bar. For more details, see Section 2.
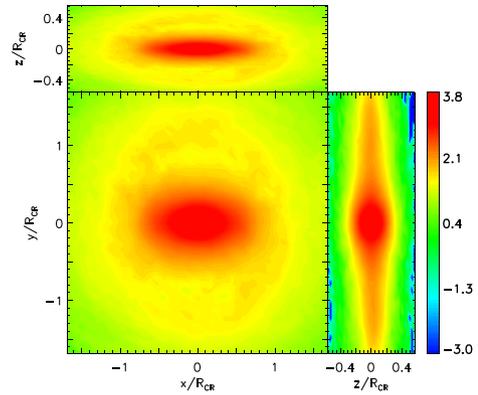

Figure 2. Face-on (bottom left), side-on (upper left) and end-on (lower right) views of the distribution of the selected 3094 orbits at time 6.0005 Gyr. The positions are normalized by the corotation radius R_{CR}.

is its azimuthal angle. The $a_m(R)$ and $b_m(R)$ are a function of the cylindrical radius. The bar strength is measured by the maximum amplitude of the relative $m = 2$ component,

$$A_2 = \max\left(\frac{\sqrt{a_2^2 + b_2^2}}{a_0}\right) \tag{4}$$

where a_0 is given by equation (2) with $m = 0$. The evolution of the bar strength and the pattern speed with time are given in Fig. 1. We note that in the time interval 6 to 10 Gyr the bar strength and the patter speed evolve little with time, so we analyse the orbits in this time interval. We selected a number of orbits visually, making sure that they were in the bar at the time of selection (6 Gyr). We then reran the simulation over the time range 6.0005–10.096 Gyr outputting only the positions, velocities and accelerations of the selected particles, but for a very large number of times (8192 outputs). We finally analysed 3094 orbits, whose initial positions at time 6.0005 Gyr are shown in Fig. 2. The full disc at the nearby time (6.005 Gyr) is also presented in Fig. 3. It is seen that the disc has a more extended range than that of the selected orbits. Here and elsewhere in this paper, the positions of these orbits are normalized by the corotation radius R_{CR}.

Figure 3. Face-on (bottom left), side-on (upper left) and end-on (lower right) views of the simulated disc at time 6.005 Gyr.

3 ORBIT CLASSIFICATION BASED ON THE FREQUENCY MAPS

The Fourier spectral analysis technique was pioneered by Binney & Spergel (1982, 1984) to classify regular and chaotic orbits, and was then extended in different forms by Laskar (1993) and CA98. The key point of this method is that regular orbits are quasi-periodic, thus the Fourier spectra should consist of discrete lines and their frequencies can be expressed as integer linear combinations of *N* fundamental frequencies (where *N* is the dimension of the model). Chaotic orbits, however, are not quasi-periodic and the corresponding frequencies of the Fourier spectra cannot be reduced to integer combinations of up to only *N* basic frequencies.

Suppose that we have N_d consecutive sampled values $z_{k'} \equiv z(t'_k)$, where $t'_k = k'\eta$, where η is sampling interval, and $k' = 0, \ldots, N_d - 1$. The discrete Fourier transform of $z_{k'}$ can be written as

$$Z_j = \frac{1}{N_d} \sum_{k'=0}^{N_d-1} z_{k'} \exp\left(-\frac{i2\pi jk'}{N_d}\right), \tag{5}$$

where $j = -N_d/2 + 1, \ldots, N_d/2$. The Fourier spectrum consists of N_d waves with amplitudes $|Z_j|$ and frequencies $\Omega_j = 2\pi j/(N_d\eta)$. We also define three amplitudes $|Z_{j,p}|$, $|Z_{j,v}|$, and $|Z_{j,pv}|$: $|Z_{j,p}|$ and $|Z_{j,v}|$ correspond to the amplitudes from the position and velocity components, respectively, and $|Z_{j,pv}|$ is given by $\sqrt{|Z_{j,p}|^2 + |Z_{j,v}|^2}/\sqrt{2}$. In this paper, we use $|Z_j|$ to represent $\sqrt{|Z_{j,p}|^2 + |Z_{j,v}|^2}$ unless stated otherwise. In order to facilitate the following discussions, we denote the time range 6.0005–8.048 Gyr as t_1, 8.0485–10.096 as t_2 and 6.0005–10.096 as t_{total} ($t_1 = t_2 = \frac{1}{2}t_{total}$).

3.1 NAFF

The NAFF was pioneered by Laskar (1990, 1993), and developed further by Papaphilippou & Laskar (1996, 1998) for both two- and three-dimensional models. The key point of NAFF is that regular orbits move on a torus-like manifold and are thus quasi-periodic.

In an integrable system with *N* degrees of freedom, the Hamiltonian $H(\mathbf{J}, \theta)$ depends only on the actions J_j, $H(J, \theta) = H(J_j)$, and the equations of motion of the system are given by

$$\dot{J}_j = 0, \qquad \dot{\theta}_j(t) = \frac{\partial H}{\partial J_j} = \omega_j(\mathbf{J}), \tag{6}$$

where θ_j are angle variables, and $j = 1, 2, \ldots, N$. The orbit in the system can be written in terms of the complex variables

$$z'_j(t) = J_j e^{i\theta_j} = z'_{j0} e^{i\omega_j t} \tag{7}$$

where $z'_{j0} = z'_j(0)$. The motions in phase space take place on the surface of tori that are products of true circles with constant radii $J_j = |z'_j(0)|$. The rate of the motions around a torus is determined by the frequency vector $(\omega_1, \omega_2, \ldots, \omega_N)$. Generally, we do not know the precise action-angle variables (J_j, θ_j), but we can find approximations (J'_j, θ'_j). In the new coordinates, the motion can be written as

$$f(t) = z'_j(t) + \sum_{k}^{\infty} A_k e^{i\langle k, \omega \rangle t} \tag{8}$$

where A_k are the complex amplitudes, and $\langle k, \omega \rangle = k_1 \omega_1 + k_2 \omega_2 + \ldots + k_N \omega_N$. In the limiting case, the coordinates (J'_j, θ'_j) are action-angle variables, and the amplitudes A_k are close to zero.

In general, a system with more than one degree of freedom is not integrable. The Hamiltonian can be expressed as a perturbation of an integrable Hamiltonian H_0,

$$H(J, \theta) = H_0(J) + \epsilon H_1(J, \theta). \tag{9}$$

If the perturbation ϵ is small, the Kolmogorov–Arnold–Moser (KAM) theorem suggests that a large fraction of the tori still exist and that the motion of most orbits is still quasi-periodic.

The frequency map analysis consists of obtaining a quasi-periodic approximation of the numerical solutions of the Hamiltonian system in equation (8) in the form of a finite number of terms without searching for an explicit transformation of coordinates in action-angle variables

$$f(t) = z'_j(t) + \sum_{k=1}^{k_{max}} A_k e^{i\langle k, \omega \rangle t} \tag{10}$$

where k_{max} is the number of terms, and A_k are of decreasing amplitude.

A regular orbit is quasi-periodic, and the complex function combining its positions and velocities $f(t) = X(t) + iV(t)$, can be expanded in a Fourier series (Binney & Tremaine 2008)

$$f(t) = \sum_{k=1}^{k_{max}} A_k \exp(i\omega_k t), \tag{11}$$

where ω_k are the linear combinations of the fundamental frequencies, $\omega_k = l_k * \omega_1 + m_k * \omega_2 + n_k * \omega_3$, A_k are the complex amplitudes and k_{max} is the number of terms. The NAFF algorithm is designed to obtain an approximate form of $f(t)$

$$f'(t) = \sum_{k=1}^{k_{max}} A'_k \exp(i\omega'_k t) \tag{12}$$

where the frequencies ω'_k and complex amplitudes A'_k can be obtained by an iterative scheme. The first frequency ω'_1 is searched by computing the maximum amplitude of $\phi(\sigma) = \langle f(t), \exp(i\sigma t) \rangle$ where the scalar product $\langle f(t), g(t) \rangle$ is given by

$$\langle f(t), g(t) \rangle = \frac{1}{T} \int_{-T/2}^{T/2} f(t) \bar{g}(t) \chi(t) dt, \tag{13}$$

where T is the time interval, $\bar{g}(t)$ is the conjugate of $g(t)$, and $\chi(t) = 1 + \cos(2\pi t/T)$ is the Hanning window function. In the NAFF routine, the location of the primary frequency corresponds to the largest amplitude among the position spectrum $|Z_{j, p}|$ and the velocity spectrum $|Z_{j, v}|$. The location of the first frequency is around the primary frequency. Once the first frequency has been found, its complex amplitude A'_1 is obtained by the orthogonal projection $A'_1 = \langle f(t), \exp(i\omega'_1 t) \rangle$. The first frequency component is subtracted and the process is restarted on the remaining part

of the $f_1(t) = f(t) - A'_1 \exp(i\omega'_1 t)$ to find the second frequency ω'_2. The process is repeated to find the third ω'_3, fourth ω'_4 and more frequency components until the residual function does not significantly decrease when subtracting the following term. The fundamental frequencies are from these selected frequencies.

For the regular orbits, the fundamental frequencies do not change with time. Therefore, the frequency drift of the fundamental frequencies in two intervals provides us the regular behaviour of the orbits. The frequency drift is defined as (Valluri et al. 2010, 2012, 2016)

$$\log(\Delta f_1) = \log \left| \frac{\omega_1(t_1) - \omega_1(t_2)}{\omega_1(t_1)} \right|, \tag{14}$$

$$\log(\Delta f_2) = \log \left| \frac{\omega_2(t_1) - \omega_2(t_2)}{\omega_2(t_1)} \right|, \tag{15}$$

$$\log(\Delta f_3) = \log \left| \frac{\omega_3(t_1) - \omega_3(t_2)}{\omega_3(t_1)} \right|, \tag{16}$$

and the frequency drift parameter $\log(\Delta f)$ is the largest value of $\log(\Delta f_1)$, $\log(\Delta f_2)$ and $\log(\Delta f_3)$. The orbit will be chaotic if the frequency drift parameter is large. Usually, a critical value $\log(\Delta f_0)$ is used to distinguish chaotic from regular orbits. If the frequency drift is smaller than the critical value $\log(\Delta f_0)$, the orbit is classified as regular, otherwise, the orbit is chaotic. It is seen that the frequency drift in this definition is a relative drift; a shortcoming of this definition occurs when the fundamental frequency is large. In particular, the accuracy of the determination of the main frequencies of the ordinary FFT is of the order of $1/T$, and the NAFF method uses a Hanning window to search for the maximum peak in the spectrum, which increases the accuracy of the main frequencies to the order of $1/T^4$ (Papaphilippou & Laskar 1996). Thus, the frequencies of the orbits can be recovered with high accuracy even for the chaotic orbits (Valluri & Merritt 1998). If the absolute values of the fundamental frequency in the first and second intervals are large, the relative value of $|(\omega_i(t_1) - \omega_i(t_2))/\omega_i(t_1)|$ will still be small. Therefore, we also use a different definition of the frequency drift, which is given by

$$\Delta F_1 = \left| \frac{\omega_1(t_1) - \omega_1(t_2)}{\delta \omega} \right|, \tag{17}$$

$$\Delta F_2 = \left| \frac{\omega_2(t_1) - \omega_2(t_2)}{\delta \omega} \right|, \tag{18}$$

$$\Delta F_3 = \left| \frac{\omega_3(t_1) - \omega_3(t_2)}{\delta \omega} \right|, \tag{19}$$

where $\delta \omega = 2\pi/(N_d \eta)$, where N_d is again the number of sampled points and η is the sampling interval. The frequency drift parameter ΔF is taken as the largest value of ΔF_1, ΔF_2 and ΔF_3. We take this frequency drift as the absolute frequency drift. A critical value ΔF_0 is used to distinguish regular orbits from chaotic ones.

Fig. 4 shows the distribution of the absolute frequency drift parameter (top) and the relative frequency drift parameter (bottom) from the NAFF method between t_1 and t_2 (solid line). It is seen that most orbits have an absolute frequency drift smaller than $2\delta \omega$. The peak of the distribution of the relative frequency drift $\log \Delta f$ is around -1, which indicates a 10 per cent frequency drift.
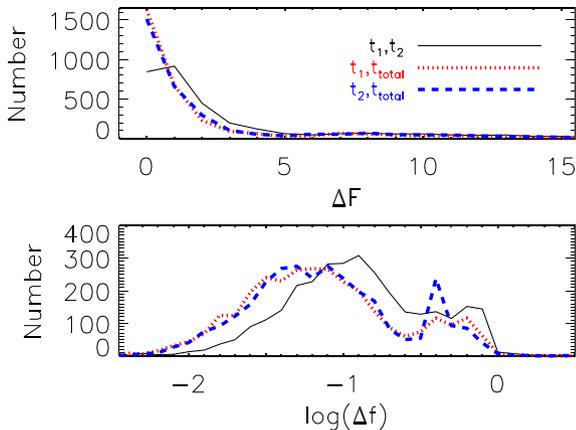
Figure 4. Distribution of the absolute frequency drift parameter ΔF (top) and the relative frequency drift parameter $\log(\Delta f)$ (bottom) for our selected 3094 orbits. The solid, dotted and dashed lines correspond to the comparison of different time ranges as labelled at the top right of the top panel.

Generally, the frequency drift can be considered between any two different intervals, therefore, we also study the cases from the t_1 time range to t_{total} and t_2 to t_{total}. In Fig. 4, we show the frequency drift parameter from time t_1 to t_{total} (dotted lines), and one from time t_2 to t_{total} (dashed lines), respectively. It is seen that most orbits have smaller absolute frequency drift parameters in $t_1 - t_{total}$ and $t_2 - t_{total}$ than those in $t_1 - t_2$, which can be explained in the following way: The frequency resolution is twice higher for time t_{total} time range than that for the t_1 and t_2 ones since we use the same time-step to output the orbits. The absolute frequency drift parameter is calculated using $\delta\omega$ rather than $0.5\delta\omega$ in cases from time t_1 to t_{total} and t_1 to t_{total}. In this paper, the orbit types are given by using the drift parameter from time t_1 to t_2 unless stated otherwise.

3.2 The CA method

The key point of CA is to find the number of the fundamental frequencies. In its initial form this method used only the position to do the Fourier transform (CA98). An updated version of the code uses the Frequency Modified Fourier Transform (FMFT; Šidlichovský & Nesvorný 1996) to extract lines, and the spectral analysis is performed on both the position and velocity component $X(t) + iV(t)$, which is similar to what is done in the NAFF scheme.

In NAFF, the frequencies are calculated sequentially and any later frequency and amplitude depend on the previous ones. Once the previous ones are found, they will not change in the subsequent steps. After $k - 1$ cycles, the k_{th} frequency is shifted from ω'_k mostly due to the existence of close frequencies which have significant amplitudes. After a number of cycles this can lead to differences of the order of several $\delta\omega$. The FMFT method consists of the NAFF process but gives a correction of frequencies via equation (36) in Šidlichovský & Nesvorný (1996). It is important to note that the frequencies and amplitudes in FMFT can change with the number of extracted lines because every frequency and amplitude are corrected by the primary selected peaks in the FFT spectrum. This is a major difference between the FMFT and the corresponding method used in NAFF (see Table 1 for an example).

The rightmost panels of Fig. 5 show 10 lines extracted by the CA method with FMFT and 10 extracted by the NAFF method in the spectra of the three (x, y, z) components for orbit 2745. It is

seen that most lines from the two methods agree, but some lines are significantly different. It is also noted that the primary frequency in the CA code is found by the largest amplitude $|Z_{j, pv}|$ (defined below equation 2) in the FFT spectrum, which is slightly different from that done in the NAFF method. For most orbits, the frequency with the largest amplitude $|Z_{j, pv}|$ is consistent with the frequency with the largest amplitude among $|Z_{j, p}|$ and $|Z_{j, v}|$. However, for some orbits this is not true. In Table 2, we show the frequencies and amplitudes of the first 20 strongest lines in the FFT spectra of orbit 1315. It is seen that the frequency with the largest $|Z_{j, pv}|$ is 78.242 571, while the frequency with the largest amplitude among $|Z_{j, p}|$ and $|Z_{j, v}|$ is 119.665 109 in the x component.

We refer the interested readers to CA98 for a full description of their technique. Here we only give a brief overview and some modifications on the new version of their code. There is a clean distinction between the main and fundamental frequencies in this new version. The main frequencies are the frequencies whose amplitudes are the maximum (or second maximum) on each coordinate. These frequencies are used to determine whether or not the orbit is resonant. The fundamental frequencies are the independent frequencies. We will take an example to illustrate this difference. If there is no integer non-zero vector (l, m, n) to satisfy $l\omega_1 + m\omega_2 + n\omega_3 = 0$, these main frequencies are independent. If the rest of the spectral lines can be expressed as the linear combinations of them, then the fundamental frequencies are the same as the main frequencies. If there are more than three independent frequencies, the number of fundamental frequencies will be 4, and thus the orbit is classified as an irregular type in CA. If there is one resonance, then the three main frequencies are not independent, the main frequencies are not the fundamental frequencies.

4 MAIN FREQUENCIES IN NAFF AND CA

There are two different conceptual frequencies in the literature, one is the fundamental frequency, and the other is the main frequency. Unfortunately, these two are sometimes confusingly used.

In NAFF, the fundamental frequencies are frequencies of the angle variables in the case of a regular orbit for which the action/angle variables exist. In that case any coordinate time series will have a spectrum made of discrete lines at frequencies that can be written as linear combinations with integer coefficients of three independent 'fundamentals frequencies'. However, unless the coordinates used are close to angle variables, there is no reason why the dominant line in one spectrum should be one of those fundamental frequencies. For box orbits, the fundamental frequencies are identified by the highest amplitude terms in the Cartesian coordinates. On the other hand, for tube orbits, the terms with the second or subsequent highest amplitudes are taken as the fundamental frequencies (Valluri & Merritt 1998).

In the CA method, the main frequencies are frequencies with the maximum or subsequent highest amplitudes of each coordinate, which is the same as the 'fundamental' frequencies in NAFF. The main frequencies in CA are used further to determine whether or not there are resonances. If there is no resonance among the main frequencies, they may be taken as fundamental frequencies too. If, however, there are resonances, then the main frequencies are used to determine one to three linearly independent fundamental frequencies for regular orbits, or more than three for irregular orbits. Therefore, the main frequencies in CA coincide with the 'fundamental' frequencies in NAFF. In the remaining of the paper, we will use the 'main' frequencies and 'fundamental' frequencies as defined in CA.

Table 1. Frequencies and amplitudes extracted from the spectrum of orbit 1315 in the x (top), y (middle) and z (bottom) components using the NAFF and CA methods with different L_{max}.

k	ω'_k (NAFF) $L_{max} = 10$	A'_k (NAFF) $L_{max} = 10$	ω'_k (NAFF) $L_{max} = 12$	A'_k (NAFF) $L_{max} = 12$	ω'_k (CA) $L_{max} = 10$	A'_k (CA) $L_{max} = 10$	ω'_k (CA) $L_{max} = 12$	A'_k (CA) $L_{max} = 12$
1	118.646975	0.087493	118.646975	0.087493	123.906921	0.205454	123.903713	0.204517
2	118.646975	0.129730	118.646975	0.129730	80.383856	0.197367	80.379904	0.197389
3	79.180676	0.189038	79.180676	0.189038	130.690324	0.222754	130.526476	0.204632
4	130.964723	0.178945	130.964723	0.178945	127.104809	0.190681	127.053323	0.188998
5	79.180569	0.187178	79.180569	0.187178	78.497611	0.215303	78.493748	0.215055
6	83.774549	0.120298	83.774549	0.120298	121.152373	0.180770	121.152083	0.180511
7	76.471528	0.057949	76.471528	0.057949	132.023087	0.174899	132.228818	0.193995
8	122.210680	0.178263	122.210680	0.178263	83.047291	0.134492	83.037662	0.134594
9	131.004247	0.159953	131.004247	0.159953	119.680380	0.142824	119.677448	0.142573
10	134.123148	0.079459	134.123148	0.079459	77.055611	0.114834	77.051043	0.114728
11			125.801781	0.195909			133.928603	0.104530
12			124.280162	0.097235			87.622990	0.072769
1	120.187879	0.289342	120.187879	0.289342	124.332263	0.447271	124.359786	0.443748
2	132.703213	0.276719	132.703213	0.276719	130.661153	0.476913	130.663652	0.476665
3	134.960731	0.192684	134.960731	0.192684	127.359892	0.430963	127.374838	0.430598
4	134.654657	0.222301	134.654657	0.222301	121.552062	0.403108	121.646264	0.390782
5	128.870117	0.408115	128.870117	0.408115	132.318424	0.453290	132.320529	0.453740
6	131.047180	0.334746	131.047180	0.334746	119.660980	0.439960	119.716928	0.440926
7	125.360971	0.463758	125.360971	0.463758	133.982798	0.242381	133.982529	0.242588
8	127.308115	0.133632	127.308115	0.133632	118.283853	0.248884	118.023337	0.341200
9	122.980739	0.414632	122.980739	0.414632	80.485974	0.132293	80.146343	0.128368
10	119.665109	0.304908	119.665109	0.304908	78.780880	0.109954	78.661243	0.110079
11			121.532408	0.054014			116.738274	0.126798
12			124.217988	0.081351			83.026349	0.084185
1	129.788437	0.160866	129.788437	0.160866	138.000765	0.345491	138.002662	0.343542
2	127.865342	0.097260	127.865342	0.097260	135.090665	0.291035	135.135194	0.290528
3	128.132109	0.182508	128.132109	0.182508	140.857289	0.264038	140.859943	0.263717
4	132.335399	0.179940	132.335399	0.179940	143.924934	0.210984	143.926056	0.210835
5	131.938453	0.189985	131.938453	0.189985	130.765206	0.327860	130.706509	0.327987
6	136.540957	0.342655	136.540957	0.342655	132.723722	0.244343	132.761358	0.232638
7	133.705729	0.138481	133.705729	0.138481	146.306622	0.202305	146.308937	0.202298
8	139.613950	0.325237	139.613950	0.325237	129.506709	0.184226	129.170063	0.259542
9	137.906023	0.064947	137.906023	0.064947	147.877606	0.156429	147.878724	0.156423
10	146.398331	0.155171	146.398331	0.155171	110.364005	0.101131	110.355605	0.101467
11			146.398154	0.192978			116.926172	0.094574
12			142.327606	0.213880			127.811826	0.115941

The first step to get the main frequencies is to extract the lines from the Fourier spectra. We use both the position and velocity components $X(t) + iV(t)$ to get the spectrum for each component. In order for positions and velocities to contribute in a comparable manner, we use a normalized, dimensionless position and velocity to do the Fourier transform. The original position and velocity are divided by R_m and V_m, respectively, where $R_m = \sqrt{\langle x^2 + y^2 + z^2 \rangle}$ and $V_m = \sqrt{\langle v_x^2 + v_y^2 + v_z^2 \rangle}$, x, y and z are the three positions, v_x, v_y and v_z are the three velocities and $\langle \cdots \rangle$ denotes the average over time along the orbit.

The detailed method to extract the spectrum is given in Laskar (2003); we refer the reader to his paper for further details. Here we just point out that the strongest spectral lines in each component are obtained using an accurate numerical technique. In NAFF, all extracted lines are sorted by amplitude in descending order. The first main frequency ω_1 corresponds to the line with the largest amplitude, the second main frequency ω_2 is the next highest peak coming from a different component and a value different from the first main frequency. The third main frequency is one of the remaining frequencies, should come from the remaining component, and should not be any linear combination of ω_1 and ω_2.

In CA, the x, y and z axes should be aligned with the major, intermediate and minor axes of the system. Then, the main frequency from each component should yield $\omega_x < \omega_y < \omega_z$, where ω_x, ω_y and ω_z are the highest peaks from the spectrum of the x, y and z components, respectively. Therefore, if the frequency from the largest peak in each component does not satisfy $\omega_x < \omega_y < \omega_z$, the CA method switches the corresponding coordinates, unless the two corresponding amplitudes are very close to each other. The first main frequency is the smallest frequency among ω_x, ω_y and ω_z. The second and third main frequencies are from the frequency components with intermediate and largest values among ω_x, ω_y and ω_z, respectively. In principle, when $\omega_x < \omega_y < \omega_z$, then the second main frequency is from the spectrum of the y component, and the third main frequency is from the spectrum of the z component. However, in practice, when ω_y is quite close to ω_x, then ω_2 is searched in descending order of amplitude in the y spectrum until ω_2 is significantly larger than ω_1. A similar treatment is adopted for the third main frequency.

Since the main frequencies are selected among the extracted lines in the spectrum in both methods, they may depend on the candidate number of the extracted lines L_{max}. Fig. 6 shows a comparison of
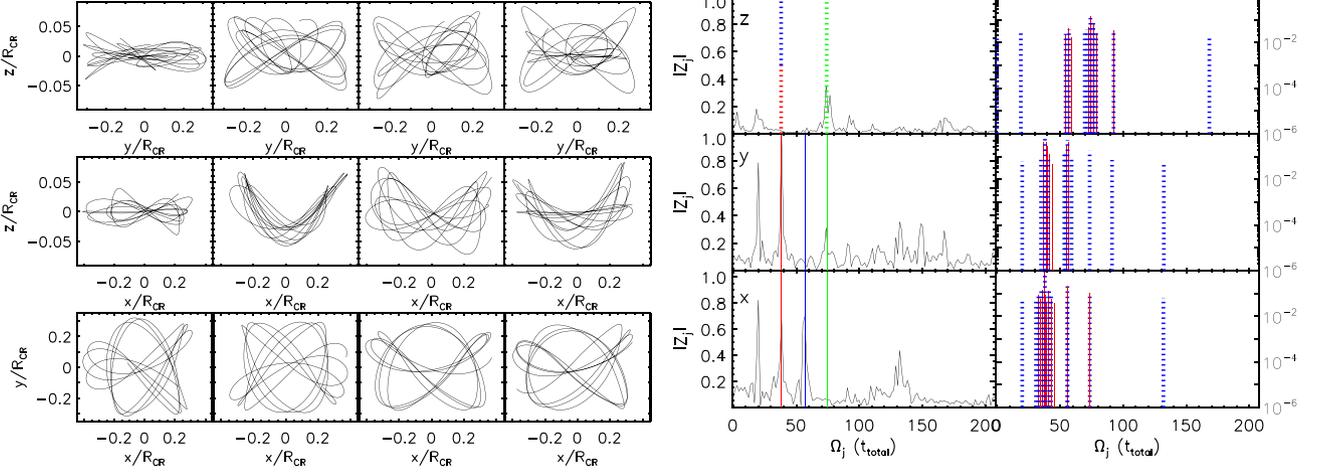
Figure 5. Left set of panels: orbit 2745. From top to bottom, the orbit in y–z, x–z and x–y planes, respectively. From left to right, the result for time 6.005–7.024, 7.0245–8.048, 8.0485–9.072, 9.0725–10.096 Gyr. Note that the scales of the ordinates and abscissas are not always the same, so as to allow for a better resolution. Right set of panels: FFT spectrum for this orbit (left) and the extracted lines (right). From top to bottom, the results for the z, y and x components, respectively. First column of the right set of panels: The red, blue and green solid lines denote the positions of ω_1, ω_2 and ω_3 from NAFF, while the corresponding dashed lines represent the main frequencies from CA method. The amplitude of the spectrum is normalized by the largest amplitude among three components. Second column of right set of panels: the red solid and blue dotted lines represent the extracted lines from NAFF and CA, respectively. [ω_1, ω_2, ω_3] =[37.980, 56.760, 74.362] (NAFF) and [ω_1, ω_2, ω_3] =[37.997, 38.004, 74.104] (CA). The ordinate of the rightmost panel is in logarithmic scale.

the main frequencies obtained with $L_{max} = 10$ and with $L_{max} = 12$ for both methods. It is seen that only a small number (<0.1 per cent) of the main frequencies in NAFF have been changed when using different values of L_{max}, while about 6 per cent of the main frequencies have been changed in CA. Here the changes in the main frequencies from $L_{max} = 10$ to $L_{max} = 12$ mean that the largest frequency difference of $|\omega_i(L_{max} = 12)/\omega_i(L_{max} = 10) - 1|$ ($i = 1$, 2, 3) is larger than 0.01. It is easy to understand these changes of the main frequencies with the increasing number of L_{max} in both the NAFF and CA methods. In the CA method, the frequencies and amplitudes of the extracted lines are corrected by the next extracted lines, therefore, the frequency and amplitude from the extracted lines are changed when L_{max} is different. In the NAFF method, the increasing number of L_{max} may give new frequencies and amplitudes. To illustrate this, we show the frequencies and amplitudes of the extracted lines in orbit 1315 for both the NAFF and the CA methods in Table 1. From the definition of the main frequencies in the two methods, we know that $\omega_1 = 79.181$ ($k = 3$ in the x component) with $L_{max} = 10$, and $\omega_1 = 125.802$ with $L_{max} = 12$ ($k = 11$) in NAFF. The shift of ω_1 in NAFF is because a new line with a large amplitude is found in the eleventh step. In the CA code, the increasing number of L_{max} changes the frequencies and amplitudes, therefore, ω_1 can be changed. In Fig. 7, we show the dependence of three main frequencies on the value of L_{max} for orbit 1315 (left) and orbit 1220 (right). It is seen that the main frequencies from NAFF will not be changed if $L_{max} \geq 12$, while there is a small fluctuation along the L_{max} value for orbit 1315. For orbit 1220, only ω_3 has been changed at $L_{max} = 36$, and will be kept as a constant with $L_{max} > 36$. In order to avoid the missing lines and save the compute time, we adopt $L_{max} = 12$ in the remainder of the paper unless stated otherwise.

In NAFF, the absolute difference between the first and second main frequencies $|\omega_i - \omega_j|$($i = 1$, 2, 3, $j = 1$, 2, 3, and $i \neq j$) must be larger than a critical value $L_{r,a}$, which we define as the critical absolute frequency difference. In CA, the parameter to distinguish two frequencies is similar to NAFF, but with the value of the relative frequency difference $|\omega_i - \omega_j|/\sqrt{\omega_i^2 + \omega_j^2}$ larger

than a critical value L_r. In order to compare the main frequencies in these two methods, we introduced a definition consistent with that of CA, i.e. $|\omega_i - \omega_j|/\sqrt{\omega_i^2 + \omega_j^2} > L_r$. In Fig. 8, we show the comparison of main frequencies from $L_r = 2 \times 10^{-4}$ and $L_r = 2 \times 10^{-3}$, where the first one is suggested by the CA method. We found that around 6 per cent and 1.5 per cent of the orbits have a different main frequency in the NAFF and the CA methods, respectively. Here we define two main frequencies as different if $|\omega_i(L_r = 2 \times 10^{-4})/\omega_i(L_r = 2 \times 10^{-3}) - 1|$ ($i = 1$, 2, 3) is larger than 0.01.

Since our orbits are extracted from a simulation, they are necessarily much noisier than those obtained from an analytic potential. In order to estimate this effect on the main frequency detection, we will vary the absolute critical value $L_{r,a}$ in the NAFF method, to check whether any lines with very small amplitude are taken as the main frequencies. In Fig. 9, we compare the main frequencies with different $L_{r,a}$, and find that even when the value of $L_{r,a}$ is increased from 10^{-6} to 1, only 22.3 per cent of the orbits change their main frequencies: the largest frequency change of $|\omega_i(L_{r,a} = 1)/\omega_i(L_{r,a} = 2 \times 10^{-6}) - 1| > 0.01$. We define nine parameters to describe the corresponding amplitude variation:

$$R_{i,a} = A_i(L_{r,a} = 10^{-4})/A_i(L_{r,a} = 10^{-6}), \qquad (20)$$

$$R_{i,b} = A_i(L_{r,a} = 10^{-2})/A_i(L_{r,a} = 10^{-6}), \qquad (21)$$

$$R_{i,c} = A_i(L_{r,a} = 1)/A_i(L_{r,a} = 10^{-6}), \qquad (22)$$

where $i = 1$, 2, 3 and A_i are the amplitudes of the main frequencies ω_i. In Fig. 10, we show the distribution of these parameters $R_{i,a}$, $R_{i,b}$ and $R_{i,c}$ in the NAFF method. We can see that some lines with low amplitude appear as new main frequencies as $L_{r,a}$ increases. However, the number of orbits for which the ratio of the amplitudes is considerably different from unity is quite small. This is true even when we change this parameter by 6 orders of magnitude, from 10^{-6} to 1 (rightmost panels). In other words, the simulation noise does not affect the main frequencies significantly.

Table 2. Frequencies and amplitudes of the first 20 strongest lines in the FFT spectra of orbit 1315. From top to bottom, the results for x, y and z components, respectively. The amplitude is normalized by the largest values of $|Z_{j,pv}|$, $|Z_{j,p}|$ and $|Z_{j,v}|$ in the x, y and z components.

	Ω_j	$|Z_{j,pv}|$	Ω_j	$|Z_{j,p}|$	Ω_j	$|Z_{j,v}|$
1	78.242571	0.376261	78.242571	0.397491	119.665109	0.441276
2	79.776739	0.341673	131.938454	0.388476	79.776739	0.372881
3	131.938454	0.341376	76.708403	0.341961	78.242571	0.353760
4	119.665109	0.322304	133.472622	0.330353	124.267613	0.323890
5	118.130941	0.306547	121.199277	0.310250	127.335949	0.322616
6	130.404285	0.290761	79.776739	0.307313	118.130941	0.321816
7	133.472622	0.277273	118.130941	0.290476	130.404285	0.309150
8	76.708403	0.261478	116.596773	0.283636	82.845075	0.303582
9	124.267613	0.260451	130.404285	0.271128	131.938454	0.286639
10	127.335949	0.230389	122.733445	0.241251	81.310907	0.239860
11	121.199277	0.222195	115.062605	0.190504	125.801781	0.220963
12	82.845075	0.216798	124.267613	0.175397	133.472622	0.211252
13	122.733445	0.206655	87.447580	0.144521	135.006790	0.203641
14	116.596773	0.203209	119.665109	0.114172	75.174235	0.171446
15	81.310907	0.171751	75.174235	0.096095	122.733445	0.164955
16	125.801781	0.157773	88.981748	0.093776	128.870117	0.159648
17	135.006790	0.144317	96.652588	0.090859	76.708403	0.140725
18	115.062605	0.143714	84.379244	0.090526	73.640067	0.120937
19	75.174235	0.138975	111.994269	0.066164	85.913412	0.116579
20	128.870117	0.113322	95.118420	0.062765	95.118420	0.105852
1	131.938454	0.817488	119.665109	1.000000	131.938454	0.918017
2	119.665109	0.736141	127.335949	0.760479	133.472622	0.801207
3	118.130941	0.689816	124.267613	0.750421	121.199277	0.707666
4	130.404285	0.663555	118.130941	0.729137	118.130941	0.648115
5	133.472622	0.647121	131.938454	0.702722	130.404285	0.630494
6	124.267613	0.600851	130.404285	0.695045	116.596773	0.629587
7	127.335949	0.539153	125.801781	0.493815	122.733445	0.570149
8	121.199277	0.510406	133.472622	0.442264	115.062605	0.445213
9	122.733445	0.455214	135.006790	0.441181	124.267613	0.398636
10	116.596773	0.449717	128.870117	0.384844	119.665109	0.289495
11	125.801781	0.356472	122.733445	0.298950	78.242571	0.257532
12	115.062605	0.327240	79.776739	0.215070	76.708403	0.225199
13	135.006790	0.312036	78.242571	0.200541	141.143462	0.178793
14	128.870117	0.276401	142.677630	0.185873	111.994269	0.175189
15	78.242571	0.230802	82.845075	0.159508	113.528437	0.162036
16	79.776739	0.185546	136.540958	0.155262	79.776739	0.150332
17	76.708403	0.171929	113.528437	0.155105	142.677630	0.148415
18	142.677630	0.168190	81.310907	0.148642	139.609294	0.130068
19	113.528437	0.158608	144.211798	0.144056	110.460101	0.126255
20	141.143462	0.132717	121.199277	0.142257	147.280134	0.122198
1	130.404285	0.595491	130.404285	0.602931	128.870117	0.611627
2	131.938454	0.461723	131.938454	0.595086	130.404285	0.587957
3	128.870117	0.436930	139.609294	0.558446	133.472622	0.420099
4	136.540958	0.428092	136.540958	0.556658	135.006790	0.410902
5	139.609294	0.394928	138.075126	0.453658	147.280134	0.392487
6	147.280134	0.393585	147.280134	0.394679	127.335949	0.314830
7	138.075126	0.321138	148.814302	0.375144	145.745966	0.313433
8	135.006790	0.310646	141.143462	0.310228	144.211798	0.286731
9	127.335949	0.307596	125.801781	0.306661	142.677630	0.277177
10	133.472622	0.305220	127.335949	0.300189	131.938454	0.268791
11	148.814302	0.285385	142.677630	0.285142	108.925933	0.257125
12	142.677630	0.281188	107.391764	0.245189	136.540958	0.238031
13	145.745966	0.271008	145.745966	0.220568	118.130941	0.185580
14	141.143462	0.220437	105.857596	0.165661	148.814302	0.148852
15	125.801781	0.218882	116.596773	0.165479	150.348470	0.135856
16	144.211798	0.208107	135.006790	0.155439	107.391764	0.133676
17	107.391764	0.197467	110.460101	0.149926	104.323428	0.129141
18	108.925933	0.184959	121.199277	0.147039	116.596773	0.111140
19	118.130941	0.143629	122.733445	0.138278	105.857596	0.108521
20	116.596773	0.140953	113.528437	0.134046	102.789260	0.099456
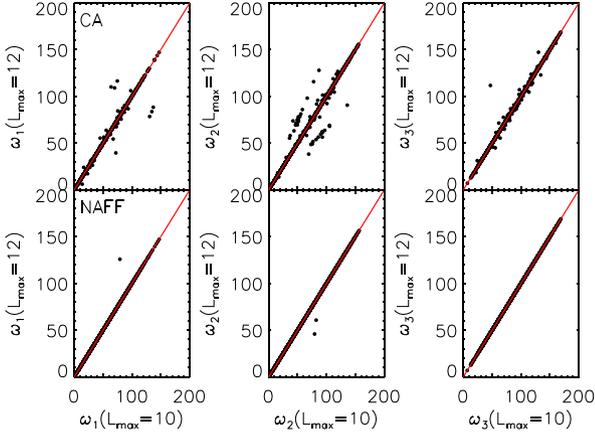
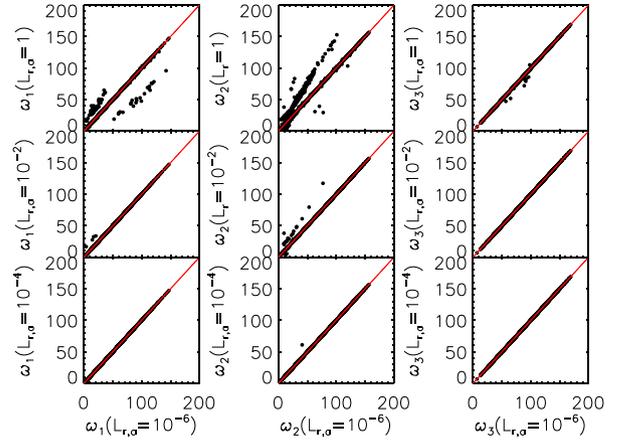**Figure 6.** Comparison of main frequencies from different values of L_{max}. The solid line represents equality of two frequencies for two different parameters L_{max} (12 and 10). The top and bottom panels represent the results from the CA and NAFF methods, respectively. The sample interval is t_{total}.
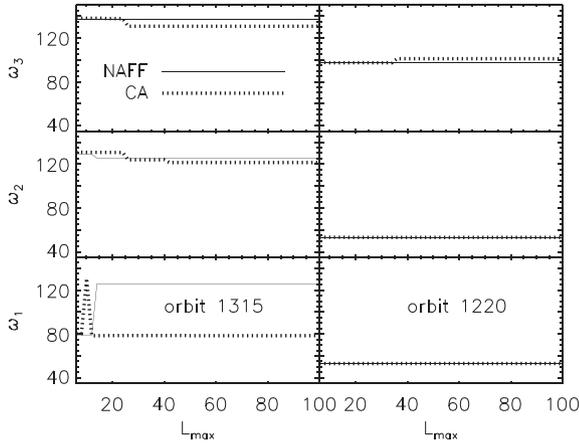

Figure 7. Dependence of three main frequencies on L_{max} for both NAFF (solid line) and CA (dotted line) for orbit 1315 (left panel) and orbit 1220 (right panel). The top, middle and bottom panels represent the results for ω_3, ω_2 and ω_1, respectively. For orbit 1220, ω_1 and ω_2 from two methods are same.
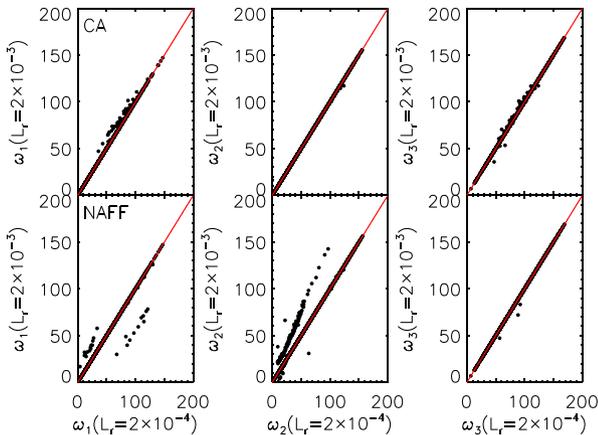
Figure 8. Comparison of main frequencies from different values of L_r. The red solid line represents equality of two frequencies for two different parameters L_r. The top and bottom panels represent the results from the CA and NAFF methods, respectively. The time interval used here is t_{total}.

Figure 9. Comparison of main frequencies from different values of $L_{r,a}$ in NAFF. The solid line represents equality of two frequencies for two parameters $L_{r,a}$. The sample interval is t_{total}.
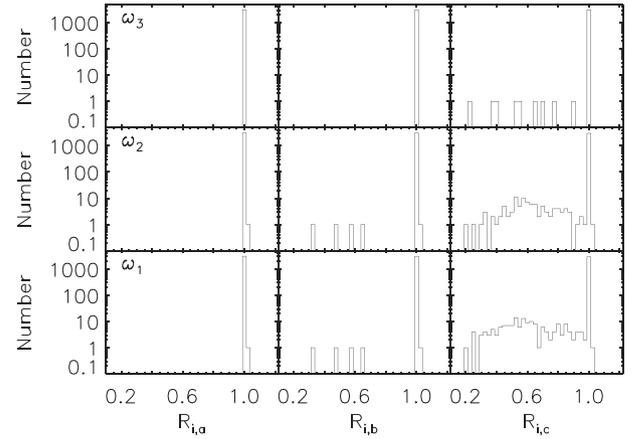
Figure 10. The distribution of the amplitude ratios. From top to bottom, the results are for ω_3, ω_2 and ω_1, respectively. The sample interval is t_{total}. The parameters $R_{i,a}$, $R_{i,b}$ and $R_{i,c}$ are defined in equations (20)–(22). Note that the scale for the ordinate is logarithmic.

We also check the distribution of the amplitude ratios in the CA method, and find results similar to those in NAFF. Therefore, the effect of the critical parameter to distinguish two frequencies is small in both methods. However, in the CA method, if we increase the value of L_r, the number of fundamental frequencies may be changed significantly, which increases the fraction of regular orbits significantly. Indeed in CA, the parameter L_r has two meanings: one is the frequency difference, which is the same as shown in our paper, while the other is the critical value determining whether an orbit is resonant, or not. In the CA code, if $|l\omega_1 + m\omega_2 + n\omega_3|/\sqrt{(l\omega_1)^2 + (m\omega_2)^2 + (n\omega_3)^2}$ is smaller than L_r, then a resonance has been found. Since the number of the fundamental frequencies depends on the resonance number of the orbits, L_r can affect the number of fundamental frequencies. In order to give a more detailed comparison of the main frequencies between the NAFF and CA methods, we adopt a relative critical value $L_r = 2 \times 10^{-4}$ in the remainder of the paper, unless otherwise indicated.

Fig. 11 shows the histogram of the ratios of the three main frequencies from both the NAFF (bottom) and CA (top) methods. It is seen that there are typical peaks in these distributions, which indicate the intrinsic orbit types in our *N*-body bar. Note that the
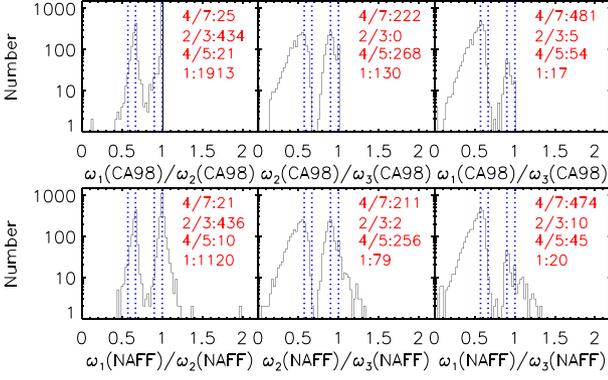
Figure 11. Histogram of the ratios of the main frequencies from the CA (top) and NAFF (bottom) methods. From left to right, the results are for the ratios with ω_1/ω_2, ω_2/ω_3, and ω_1/ω_3, respectively. From left to right, the vertical dashed lines represent ratios with 4/7, 2/3, 4/5 and 1, respectively. The sample interval is t_{total}. The ratio and the corresponding orbit numbers are indicated in the top-right corner of each panel.
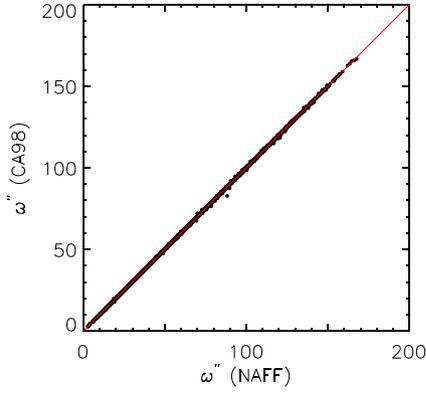

Figure 12. Comparison of one similar main frequency from NAFF with that from CA. The solid line represents equality of two frequencies from these two methods. The sample interval is t_{total}.

ordinate is in a logarithmic scale, which means that the peaks are very high, i.e. that many orbits are in families with well-defined frequency ratios. For both methods, the face-on view, (x, y), has two clear peaks. The highest peak is for 1:1, and the second highest for 2:3, the two having amplitudes of 1120 and 436 in NAFF, 1913 and 434 in CA98. The two edge-on views, (y, z) and (x, z), also have two clear peaks, one at 4:5 and the other at 4:7. The implications of this result will be discussed elsewhere.

We define nine parameters to check whether a main frequency agrees in the two methods:

$$\delta f_1^{ij} = \left| \frac{\omega_i(\text{NAFF})}{\omega_j(\text{CA})} - 1 \right|, \tag{23}$$

with $i = 1, 2, 3$ and $j = 1, 2, 3$. We take the minimum value of δf_1^{ij} as δf_1. If δf_1 is small, then at least one main frequency from CA is consistent with one from NAFF. The corresponding frequency to δf_1 is defined as ω''. We find that 97 per cent of the orbits have the minimum δf_1 smaller than 0.01; in other words, these orbits have at least one similar main frequency from the two methods, which can also be seen from the comparison of one similar main frequency in Fig. 12. Then we define 18 parameters to check two
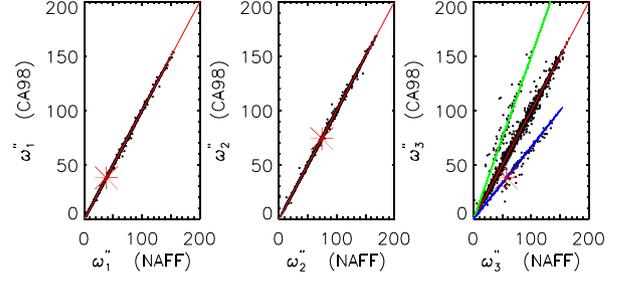
Figure 13. Comparison of the three main frequencies from the NAFF and CA methods. The red solid line represents the equality of two frequencies from the two methods. From left to right, the results are for ω_1'', ω_2'' and ω_3'', respectively. In the right panel, the green and blue solid lines present $Y = AX$ with $A = 3/2$ and $A = 2/3$, respectively. The sample interval is t_{total}. The red asterisk symbol denotes the location of orbit 2745 in each panel.

main frequencies agree from two methods, these parameters are given as

$$\delta f_2^{ij,i'j'} = \left| \frac{\omega_i(\text{NAFF})}{\omega_j(\text{CA})} - 1 \right| + \left| \frac{\omega_{i'}(\text{NAFF})}{\omega_{j'}(\text{CA})} - 1 \right|, \tag{24}$$

with $i = 1, 2, 3$, $j = 1, 2, 3$, $i' = 1, 2, 3$, $j' = 1, 2, 3$, and $i' \neq i$, $j' \neq j$. The minimum value of $\delta f_2^{ij,i'j'}$ is defined as δf_2. Two main frequencies agree in the two methods if δf_2 is smaller than a critical value $\delta f_{2,0}$. If the remaining main frequencies from two methods are also close (the frequency difference is smaller than $\delta f_{2,0}/2$), then all three main frequencies are in agreement. The first two identical main frequencies are defined as ω_1'' and ω_2'', and the remaining main frequency as ω_3''. We find 88 per cent orbits have two frequencies in agreement and 39 per cent orbits have three frequencies in agreement from two methods if $\delta f_{2,0} = 0.02$. If we increase $\delta f_{2,0}$ to 0.1, then 99 per cent of the orbits have two frequencies in agreement and 80 per cent of the orbits have three frequencies in agreement between the two methods. In other words, most orbits have an average difference in the main frequency smaller than 5 per cent.

In Fig. 13, we show the comparison of the three main frequencies from the two methods. The two first panels, referring to the two first frequencies, show a close equality, with all points distributed very close to the diagonal. The third panel, referring to the third frequency, has a different structure. About 80 per cent of the points (2458 orbits) are around the diagonal, but with a considerably larger spread than for the first and second frequency. This may argue that this third frequency is less accurately defined than the other two. Note also that a considerable number of orbits (144 orbits, 5 per cent) are located at the wings along the green and blue solid lines which follow $Y = AX$ with $A = 3/2$ (green) or $A = 2/3$ (blue), respectively. This could be due to a badly recognized third frequency.

As shown in Valluri et al. (2010), the accuracy of the frequency analysis decreases significantly when orbits were integrated for less than 20 oscillation periods, therefore, it is interesting to compare the main frequencies from the NAFF method with those from the CA method for orbits with more than 20 oscillation periods. In the top panel of Fig. 14, we show the fraction of our orbits with fixed oscillation periods. We find that 70 per cent orbits have more than 20 oscillation periods. In the bottom panel of Fig. 14, we present the histogram of the oscillation periods. It is noted that the distribution peaks around 20. Therefore, the output interval for most orbits in our sample is reasonable for the frequency analysis. Fig. 15 shows that the fraction of orbits having three frequencies in agreement ($\delta f_{2,0} = 0.1$) from the two methods increases strongly with the
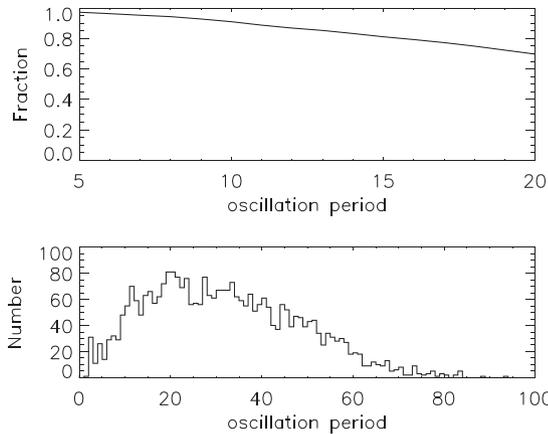
Figure 14. Top: fraction of the orbits having completed at least a given number of oscillation periods during the time we follow our simulation, as a function of this number of oscillation periods. Bottom: histogram of the oscillation periods.
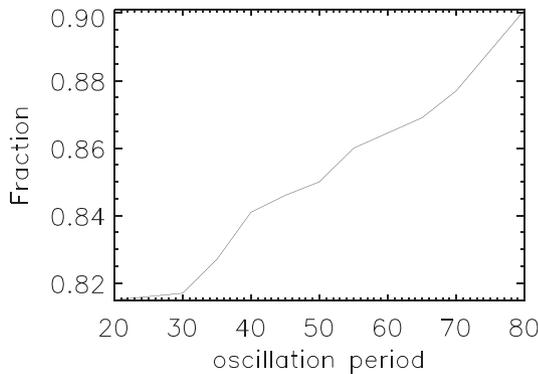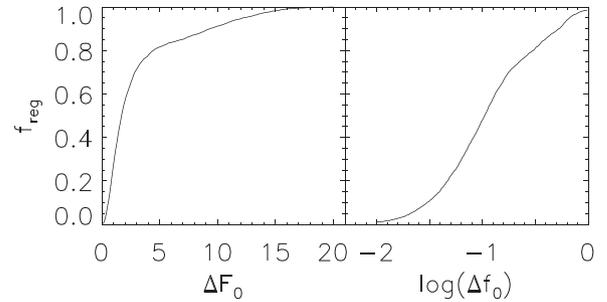

Figure 15. Dependence of the fraction of the orbits with the same main frequencies in both NAFF and CA methods on the orbit oscillation periods.

number of orbit oscillation periods. We find that, for 90 per cent of the orbits having undergone at least 80 oscillation periods, the three frequencies as calculated by the CA and NAFF methods agree. On the other hand, for orbits which have less than five oscillation periods, only 39 per cent have three frequencies in agreement between two methods.

5 FRACTION OF REGULAR ORBITS AS OBTAINED FROM NAFF AND CA

Once we have the main frequencies, NAFF classifies orbits as regular or chaotic using the frequency drift. CA classifies the orbits by finding the number of the fundamental frequencies. Fig. 16 shows the dependence of the fraction of regular orbits on the absolute critical frequency drift parameter (left panel) and the relative critical frequency drift parameter (right panel) from the NAFF method. It is seen that the fraction of regular orbits strongly depends on the critical frequency drift value, but it is difficult to give a reasonable choice.

In order to compare the ranking of the various orbits in regularity by two kinds of the critical value in the NAFF method, we rank all orbits as a function of their ΔF values. The ranking is defined as $r_{\Delta F}$. The most regular orbit will have $r_{\Delta F} = 1$ and the most chaotic one $r_{\Delta F} = 3094$. We then rank 3094 orbits as function of their $\log(\Delta f)$ values, which is called $r_{\Delta f}$. Again, the most regular orbit

Figure 16. Dependence of the fraction of regular orbits on the critical frequency drift parameter from NAFF. Left: for the absolute frequency drift. Right: for the relative frequency drift.
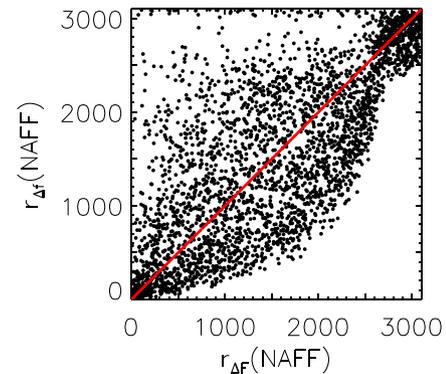

Figure 17. Comparison of the ranking of the orbits in regularity by ΔF and $\log(\Delta f)$. The red solid line represents the equality of the two rankings from $r_{\Delta F}$ and $r_{\Delta f}$.

will have $r_{\Delta f} = 1$ and the most chaotic one $r_{\Delta f} = 3094$. Fig. 17 shows the comparison of the ranking of the orbits in regularity by ΔF and $\log(\Delta f)$. We find that only 727 orbits have similar rankings in $r_{\Delta F}$ and $r_{\Delta f}$ ($|r_{\Delta f}/r_{\Delta F} - 1| \leq 0.1$). For most orbits, however, there is a large dispersion between $r_{\Delta F}$ and $r_{\Delta f}$.

In CA, an orbit is classified by the number of the fundamental frequencies. An orbit is irregular if it has more than three independent fundamental frequencies, otherwise it is regular. In this method, there are two important parameters L_r and I_n. The former is used to determine whether the two main frequencies are the same, and whether the main frequencies are at resonance, while the latter one is the maximum integer for searching linear independence of the fundamental frequencies (see Section 4). Although the main frequencies weakly depend on the parameter L_r, the number of fundamental frequencies strongly depends on it, thus affecting the fraction of regular orbits. In the left panel of Fig. 18, this fraction increases with the increasing value of L_r. If L_r is larger than 10^{-4}, most orbits are regular. In the right panel of Fig. 18, we show the dependence of the fraction of regular orbits on the parameter I_n. It is noted that most orbits are regular if I_n is larger than 25. $I_n = 35$ is usually chosen in order to classify correctly a large set of orbits coming from selected known analytic potentials (Carpintero, private communication). In the bar system, nearly all orbits are regular if $I_n = 35$.

The upper panel of Fig. 19 shows the number of orbits with more than 50 oscillations. It is a decreasing function of radius, as expected, because the inner orbits have, on average, shorter orbital periods than the outer ones. All orbits with more than 50 oscillations have the average radius $\langle R/R_{CR} \rangle$ smaller than 0.2. The lower panel of Fig. 19 shows the correlation between the fraction of regular orbits
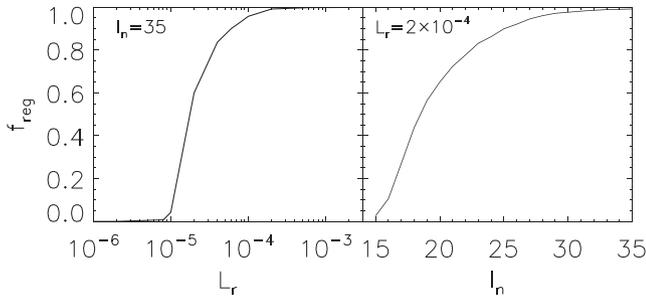
Figure 18. Dependence of the fraction of regular orbits on the parameters L_r (left panel) and I_n (right panel) in CA. For the left and right panels, the parameters I_n and L_r are fixed at 35, and 2×10^{-4}, respectively.
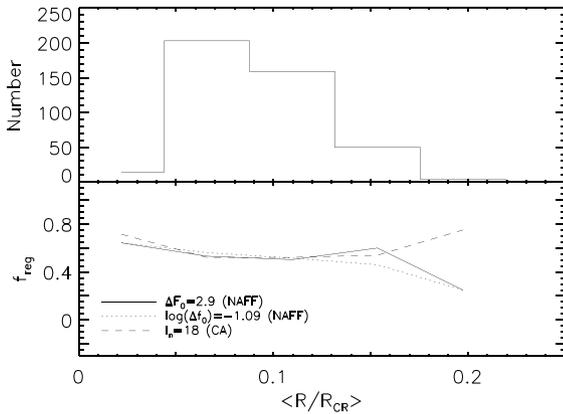

Figure 19. Top: number distribution of the orbits with more than 50 oscillation periods. Bottom: fraction of regular orbits along the average radius of the orbits for orbits with more than 50 oscillation periods. The solid, dotted and dashed lines represent the results from the absolute critical value in NAFF, relative critical value in NAFF and CA, respectively. The different lines represent the results with the different parameters in two methods. The region with $\langle R/R_{CR} \rangle$ beyond 0.2 is ignored because there are no orbits with more than 50 oscillation periods.

and the average orbit radius for orbits with more than 50 oscillations for the two methods with different parameters. For $\Delta F_0 = 2.9$ or $\log(\Delta f_0) = -1.09$ in NAFF, and $I_n = 18$ in CA, we find in general very good agreement between all methods, with a fraction of regular orbits around 53 per cent.

It seems that the regular fraction along the radius from NAFF with $\log(\Delta f_0) = -1.09$ is consistent with that from CA with $I_n = 18$ if $\langle R/R_{CR} \rangle$ is smaller than 0.18. If, however, we compare the orbit types from the two methods one by one, we find a small decrease, so that only 47 per cent of the orbits have the same type in both NAFF and CA methods. When we compare the two NAFF methods, we find that a very large fraction, 95 per cent, have the same types when we use $\Delta F_0 = 2.9$ and $\log(\Delta f_0) = -1.09$ in NAFF.

If we take $\log(\Delta f_0) = -1.09$ and consider the frequency drift parameter only in the x, y, and z components, respectively, then the regular orbit fractions are 56.2 per cent, 52.2 per cent and 72.8 per cent. If we consider the frequency drift parameter in two components, x and y, x and z, y and z, then the regular orbit fractions with $\log(\Delta f_0) = -1.09$ are 43.2 per cent, 50.7 per cent and 46.7 per cent, respectively. Therefore, the z component is most regular, while the y component is most chaotic in the bar system. This is similar to the fact that the intermediate tube orbits are unstable in the triaxial system (e.g. Merritt & Fridman 1996; Binney & Tremaine 2008).
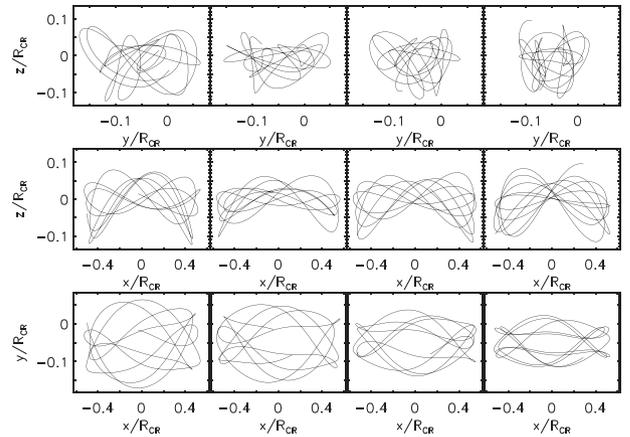
Figure 20. Same as the left panel of Fig. 5, but for orbit 160, an orbit looks regular in the x–y and x–z planes, but chaotic in the y–z plane.
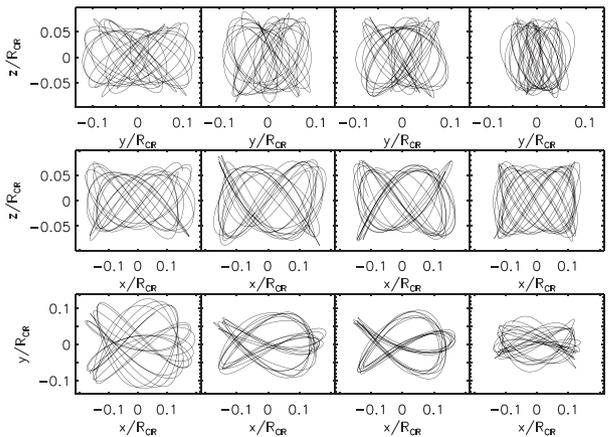
Figure 21. Same as the left panel of Fig. 5, but for orbit 865, an orbit being regular in each interval, but the shape changing with time.

6 DISCUSSION

It seems difficult to give definite values of ΔF_0 and $\log(\Delta f_0)$ in NAFF, and L_r and I_n in CA to classify orbits, but we can attempt to do this by selecting some likely regular and chaotic orbits. We use 196 orbits which have the same main frequencies from the NAFF and CA methods, and have a small frequency drift $\Delta F < 0.5$. We find that when we choose $I_n \geq 30$ and $L_r = 2 \times 10^{-4}$, most of these orbits are regular in the CA method. Even so, a few of these orbits are still irregular when we take $I_n = 30$. For example, as shown in Fig. 20, orbit 160 is a regular orbit in NAFF, but we find there are some chaotic property in the y–z plane and this could explain why CA classifies it irregular.

Next we select 40 orbits which have the same main frequencies from the NAFF and CA methods, but with large frequency drift $\Delta F > 9.3$. Most of them are irregular when we take $I_n = 16$, but orbits such as orbit 865 are still regular in the CA method. From Fig. 21, usually this orbit is regular in each interval, but the shape changes with time. Since the three main frequencies are independent and no extra fundamental frequencies are found, the CA method classifies it as a regular box orbit. On the other hand, if we use the frequency drift method to classify it, it will be classified as irregular. This frequency drift, however, could perhaps be due to the slight potential changes with time and may not necessarily be due to the fact that the orbit is irregular.

There is a further point related to the evolution of the potential. Namely, we find that the smallest ΔF among the full 3094 orbits is 0.016, while the resolution of the main frequencies is usually 10^{-4} to 10^{-3}. Thus, even the smallest ΔF is still larger than the frequency resolution. If we take $\Delta F_0 = 0.01$, then every orbit is chaotic in NAFF; a small I_n in CA with $L_r = 2 \times 10^{-4}$ can give similar results, so we can say both methods are in good agreement, but this is only an extreme case. Compared with the CA method, the results of NAFF only weakly depend on L_r and L_{max}. For the parameter L_{max}, if we do not take into account CPU time limits, we can make it as large as possible. Also the I_n value may have to be chosen differently for different potentials in the CA method. The advantage of the CA method is that it can give independent fundamental frequencies of orbits, which can yield more detailed information about regular orbits.

7 SUMMARY AND CONCLUSIONS

Individual particle orbits are the backbone of any structure. It is thus important for understanding the formation and evolution of this structure to know whether the orbits that constitute it are chaotic or regular and, in the latter case, what family they are associated with. Bars, in particular, are a favourite field for such tests and thus many studies have addressed the orbital structure in bars. Most of them, however, use an analytic potential and are thus not very realistic (see e.g. Athanassoula 2016, for a review). A further disadvantage of such studies is that it is not trivial to choose the initial conditions for the orbits and the result can depend critically on this choice. Instead, we used here orbits taken directly from the simulation. This means that they have very realistic potentials, but at the expense of some noise and, particularly, some evolution of the potential.

As a first step towards understanding the orbital structure in bars, we compare in this paper two methods: the NAFF method of Laskar (1990) and the method of CA98.

We show how the main frequencies depend on the maximum extracted line number L_{max} and on the parameter to distinguish two main frequencies L_r. We find that only a small number (<0.1 per cent) of the main frequencies in NAFF have been changed when using different values of L_{max}, while about 6 per cent of the main frequencies have been changed in CA. If we change L_r from 2×10^{-4} to 2×10^{-3}, then around 6 per cent and 1.5 per cent of the orbits have a different main frequency in the NAFF and CA methods, respectively.

We find that, at least for our case, the main frequencies calculated by the two methods are in good agreement provided we use the same definitions and values for L_{max} and L_r: for 80 per cent of the orbits the differences between the results of the two methods are less than 5 per cent for all three main frequencies. We also find that there are two clear peaks in the histogram of the ratios of the three main frequencies in both methods. The highest peak is 1:1, and the second highest is 2:3 for the face-on view (x, y). The two edge-on views, (y, z) and (x, z), also have two clear peaks, one at 4:5 and the other at 4:7.

We find that the fraction of the regular orbits strongly depends on two parameters L_r and I_n in the CA method. The former is used to determinate whether the two frequencies are the same and whether there are resonances among the main frequencies. The fraction of the regular orbits increases with increasing L_r or I_n. In the NAFF methods, the fraction of the regular orbits strongly depends on the critical frequency drift parameter. The regular fraction is increased with increasing this parameter. However, it is difficult to give certain values of these parameters in both methods. The fact that there is no abrupt change from chaotic to regular reflects the fact that there is stickiness and confined chaos. We also find that, for a given particle, in general the projection of its motion along the bar minor axis is more regular than the other two projections, while the projection along the intermediate axis is the least regular.

Increasing the number of particles in the simulation will decrease the noise. In a future paper we plan to use a simulation with a considerably larger number of particles, to determine how noise may influence the results.

REFERENCES

Athanassoula E., 2002, ApJ, 569, L83
Athanassoula E., 2003, MNRAS, 341, 1179
Athanassoula E., 2005, Ann. New York Acad. Sci., 1045, 168
Athanassoula E., 2013, Falcón-Barroso J., Knapen J. H., eds, Secular Evolution of Galaxies. Cambridge University Press, Cambridge, UK, p. 305
Athanassoula E., 2016, Galactic Bulges, 418, 391
Athanassoula E., Machado R. E. G., Rodionov S. A., 2013, MNRAS, 429, 1949
Benettin G., Galgani L., Strelcyn J.-M., 1976, Phys. Rev. A, 14, 2338
Benettin G., Galgani L., Giorgilli A., Strelcyn J.-M., 1978, Academie des Sciences Paris Comptes Rendus Serie B Sciences Physiques, 286, 431
Binney J., Spergel D., 1982, ApJ, 252, 308
Binney J., Spergel D., 1984, MNRAS, 206, 159
Binney J., Tremaine S., 2008, Galactic Dynamics, 2nd edn, Princeton University Press, Princeton
Bryan S. E., Mao S., Kay S. T., Schaye J., Dalla Vecchia C., Booth C. M., 2012, MNRAS, 422, 1863
Buta R. J. et al., 2010, ApJS, 190, 147
Buta R. J. et al., 2015, ApJS, 217, 32
Carpintero D. D., Aguilar L. A., 1998, MNRAS, 298, 1 (CA98)
Carpintero D. D., Muzzio J. C., Vergne M. M., Wachlin F. C., 2003, Celest. Mech. Dyn. Astron., 85, 247
Carpintero D. D., Muzzio J. C., Navone H. D., 2014, MNRAS, 438, 2871
Ceverino D., Klypin A., 2007, MNRAS, 379, 1155
Contopoulos G., Papayannopoulos T., 1980, A&A, 92, 33
Gajda G., Lokas E. L., Athanassoula E., 2015, preprint (arXiv:1511.04253)

Gajda G., Lokas E. L., Athanassoula E., 2016, ApJ, preprint (arXiv:1606.00322)

Häfner R., Evans N. W., Dehnen W., Binney J., 2000, MNRAS, 314, 433

Hernquist L., 1993, ApJS, 86, 389

Laskar J., 1990, Icar, 88, 266

Laskar J., 1993, Phys. D Nonlinear Phenomena, 67, 257

Laskar J., 2003, preprint (arXiv:math/0305364)

Lee G.-H., Park C., Lee M. G., Choi Y.-Y., 2012, ApJ, 745, 125

Machado R. E. G., Manos T., 2016, MNRAS, 458, 3578

McMillan P. J., Binney J. J., 2008, MNRAS, 390, 429

Manos T., Athanassoula E., 2011, MNRAS, 415, 629

Manos T., Machado R. E. G., 2014, MNRAS, 438, 2201

Martinez-Valpuesta I., Shlosman I., Heller C., 2006, ApJ, 637, 214

Merritt D., Fridman T., 1996, ApJ, 460, 136

Papaphilippou Y., Laskar J., 1996, A&A, 307, 427

Papaphilippou Y., Laskar J., 1998, A&A, 329, 451

Rodionov S. A., Athanassoula E., Sotnikova N. Y., 2009, MNRAS, 392, 904

Šidlichovský M., Nesvorný D., 1996, Celest. Mech. Dyn. Astron., 65, 137

Skokos C., 2001, J. Phys. A Math. Gen., 34, 10029

Skokos C., Antonopoulos C., Bountis T. C., Vrahatis M. N., 2004, J. Phys. A Math. Gen., 37, 6269

Skokos C., Bountis T. C., Antonopoulos C., 2007, Phys. D Nonlinear Phenomena, 231, 30

Springel V., 2005, MNRAS, 364, 1105

Springel V., Yoshida N., White S. D. M., 2001, New Astron., 6, 79

Valluri M., Merritt D., 1998, ApJ, 506, 686

Valluri M., Debattista V. P., Quinn T., Moore B., 2010, MNRAS, 403, 525

Valluri M., Debattista V. P., Quinn T. R., Roškar R., Wadsley J., 2012, MNRAS, 419, 1951

Valluri M., Shen J., Abbott C., Debattista V. P., 2016, ApJ, 818, 141

Voglis N., Kalapotharakos C., Stavropoulos I., 2002, MNRAS, 337, 619

Voglis N., Harsoula M., Contopoulos G., 2007, MNRAS, 381, 757

Wang Y., Zhao H., Mao S., Rich R. M., 2012, MNRAS, 427, 1429

Wang Y., Mao S., Long R. J., Shen J., 2013, MNRAS, 435, 3437

Wozniak H., Michel-Dansac L., 2009, A&A, 494, 11

Zhao H. S., 1996, MNRAS, 283, 149

This paper has been typeset from a TEX/LATEX file prepared by the author.